The HOPS/class C Vps complex tethers membranes by binding to one Rab GTPase in each apposed membrane

Ruoya Ho and Christopher Stroupe
Department of Molecular Physiology and Biological Physics and Center for Membrane Biology, University of Virginia School of Medicine, Charlottesville, VA 22908

ABSTRACT **Many Rab GTPase effectors are membrane-tethering factors, that is, they physically link two apposed membranes before intracellular membrane fusion. In this study, we investigate the distinct binding factors needed on apposed membranes for Rab effector–dependent tethering. We show that the homotypic fusion and protein-sorting/class C vacuole protein-sorting (HOPS/class C Vps) complex can tether low-curvature membranes, that is, liposomes with a diameter of ~100 nm, only when the yeast vacuolar Rab GTPase Ypt7p is present in both tethered membranes. When HOPS is phosphorylated by the vacuolar casein kinase I, Yck3p, tethering only takes place when GTP-bound Ypt7p is present in both tethered membranes. When HOPS is not phosphorylated, however, its tethering activity shows little specificity for the nucleotide-binding state of Ypt7p. These results suggest a model for HOPS-mediated tethering in which HOPS tethers membranes by binding to Ypt7p in each of the two tethered membranes. Moreover, because vacuole-associated HOPS is presumably phosphorylated by Yck3p, our results suggest that nucleotide exchange of Ypt7p on multivesicular bodies (MVBs)/late endosomes must take place before HOPS can mediate tethering at vacuoles.**

Monitoring Editor
Francis A. Barr
University of Oxford

Received: Apr 18, 2014
Revised: May 13, 2015
Accepted: May 15, 2015

INTRODUCTION

Membrane fusion is required for intracellular vesicular traffic and for regulation of organelle size and copy number (Wickner and Schekman, 2008). Before membranes can fuse, however, they must tether, that is, physically associate without merging lipid bilayers. Tethering has been proposed to be carried out by "tethering factors" (Waters and Pfeffer, 1999), which typically belong to one of two classes: homodimeric proteins with long regions of predicted coiled-coil structure, and large multisubunit protein complexes (Sztul and Lupashin, 2006).

In this study, we investigate the mechanism of Rab GTPase–dependent membrane tethering. Many tethering factors are effectors for Rab GTPases, that is, they bind to Rabs that are in their active, GTP-bound forms (Novick *et al.*, 2006). Rab GTPases themselves associate with membranes via aliphatic isoprenyl groups covalently linked to carboxy-terminal cysteines (Calero *et al.*, 2003). Particular Rab GTPases are found on specific organelles—in some cases, in distinct subdomains on an organelle (Sönnichsen *et al.*, 2000)—which has led to the proposal that Rabs help define membrane identity (Pfeffer, 2001). Many Rab GTPases play this role by recruiting specific tethering factors, while other Rabs regulate other aspects of intracellular traffic, for example, vesicle budding and motor-dependent translocation (Grosshans *et al.*, 2006). The first evidence for a role of Rab GTPases in tethering was the finding that a dominant-negative mutation in Sec4p, a Rab needed for secretion in the budding yeast *Saccharomyces cerevisiae*, causes buildup of untethered secretory vesicles (Walworth *et al.*, 1989). Later it was shown that antibodies against the yeast vacuolar Rab Ypt7p block in vitro tethering of purified vacuoles (Mayer and Wickner, 1997). Ypt7p's effector, the six-subunit homotypic fusion and protein-sorting/class C vacuole protein-sorting (HOPS/class C Vps) complex, is

This article was published online ahead of print in MBoC in Press (http://www.molbiolcell.org/cgi/doi/10.1091/mbc.E14-04-0922) on May 20, 2015.

Address correspondence to: Christopher Stroupe (chris.stroupe@virginia.edu).

Abbreviations used: βOG, *n*-β-octylglucopyranoside; ALPS, amphipathic lipid–packing sensor; class C Vps, class C vacuole protein-sorting; fluorescein–DHPE, *N*-fluorescein–5-thiocarbamoyl-1,2-dihexadecanoyl-*sn*-glycero-phosphatidylethanolamine; GEF, guanine nucleotide exchange factor; HOPS, homotypic fusion and protein-sorting; MVBs, multivesicular bodies; p-HOPS, phosphorylated HOPS; PMT, photomultiplier tube; POPC, 1-palmitoyl-2-oleoyl-*sn*-glycero-3-phosphatidylcholine; POPS, 1-palmitoyl-2-oleoyl-*sn*-glycero-3-phosphatidylserine; Texas Red–DHPE, Texas Red–1,2-dihexadecanoyl-*sn*-glycero-3-phosphatidylethanolamine.

Supplemental Material can be found at:
http://www.molbiolcell.org/content/suppl/2015/05/18/mbc.E14-04-0922v1.DC1.html

also required for vacuole tethering (Stroupe *et al.*, 2006). Together purified Ypt7p and HOPS are sufficient for tethering of reconstituted proteoliposomes (Hickey and Wickner, 2010).

A common feature of tethering factors is their ability to interact with multiple membrane-associated proteins. For example, golgins are a diverse family of Golgi-localized coiled-coil tethers with binding sites for numerous Rab GTPases in their coiled-coil regions (Munro, 2011). Many golgins also contain Arf GTPase–binding GRAB or Arl GTPase–binding GRIP domains at their C-termini (Munro, 2011). Similarly, the HOPS complex can bind to two molecules of Ypt7p via its Vps39p and Vps41p subunits (Bröcker *et al.*, 2012). HOPS also interacts with soluble *N*-ethylmaleimide–sensitive factor attachment protein receptor (SNARE) proteins and SNARE complexes via its Vps33p subunit, which is a member of the SNARE-binding Sec1/munc18 family (Price *et al.*, 2000; Sato *et al.*, 2000; Collins *et al.*, 2005; Lobingier and Merz, 2012). An interaction between HOPS and an Arl GTPase has also been reported (Garg *et al.*, 2011). Other tethering complexes—for example, exocyst, COG, TRAPP I/II/III, GARP/VFT, and DSL—have similar intermolecular interactions and are reviewed elsewhere (Bonifacino and Hierro, 2011; Meiringer *et al.*, 2011; Heider and Munson, 2012; Yu and Liang, 2012; Willett *et al.*, 2013). This shared attribute of tethering factors, the potential to bind simultaneously to multiple factors, suggests that Rab-dependent tethering occurs when a Rab effector tethering factor binds a Rab GTPase in one membrane and a second protein—either a Rab or another factor—in an apposed membrane.

Historically, investigation of this possible mechanism has been hampered by the lack of an assay for tethering of membranes with differing protein composition. Past assays for tethering relied on measurement of the size of tethered liposome clusters by light (Stroupe *et al.*, 2009) or electron microscopy (Drin *et al.*, 2008) or by dynamic light scattering (Araç *et al.*, 2006; Drin *et al.*, 2008; Lo *et al.*, 2011). More recently, membrane tethering and fusion assays based on colocalization of membranes labeled with differently colored fluorophores have been reported (Cottam *et al.*, 2014; Tamura and Mima, 2014). Such assays offer the possibility of distinguishing the proteins needed on distinct membranes in order for these membranes to tether.

In this study, then, we have assayed for heterotypic membrane tethering via colocalization of reconstituted proteoliposomes tagged with green or red fluorophores, which we measure by quantitative confocal fluorescence microscopy. We have used this assay to test the hypothesis that HOPS can tether membranes by simultaneously binding to a Rab GTPase in each of the apposed membranes. We further tested the effect of HOPS phosphorylation by the vacuolar casein kinase I, Yck3p, on the specificity of HOPS-mediated tethering for the nucleotide-bound state of Ypt7p. Our results allow us to propose a model for tethering of vacuoles with multivesicular bodies (MVBs)/late endosomes, and with other vacuoles, before membrane fusion.

RESULTS AND DISCUSSION

We began by incorporating purified Ypt7p (Stroupe *et al.*, 2009) into liposomes extruded through a membrane with 100-nm pores (see *Materials and Methods*). The liposomes had a composition of 95.5 mol% 1-palmitoyl-2-oleoyl-*sn*-glycero-3-phosphatidylcholine (POPC), 4.4% 1-palmitoyl-2-oleoyl-*sn*-glycero-3-phosphatidylserine (POPS), and either Texas Red–1,2-dihexadecanoyl-*sn*-glycero-3-phosphatidylethanolamine (Texas Red–DHPE; 0.1 mol%) or *N*-fluorescein–5-thiocarbamoyl-1,2-dihexadecanoyl-*sn*-glycero-phosphatidylethanolamine (fluorescein–DHPE; 0.1 mol%). This mole fraction of POPS is equal to that measured previously in yeast vacuoles (Zinser *et al.*, 1991).

We measured Ypt7p incorporation by SDS–PAGE and Coomassie brilliant blue staining (Figure 1A). Final Ypt7p incorporation was always 1:100–1:150 (Figure 1A and unpublished data), starting from a 1:100 Ypt7p:lipid molar ratio in incorporation reactions. Assuming 80 nm^2 surface area per lipid (Burke *et al.*, 1973) and a 100-nm liposome diameter (see next paragraph), this corresponds to ~25,000 Ypt7p molecules per square micrometer. This ratio is much higher than that on purified yeast vacuoles, which has been measured as ~1:200,000 Ypt7p:lipid or ~12.5 Ypt7p molecules per μm^2 for 2-μm-diameter vacuoles (Zick *et al.*, 2014). Another estimate of vacuolar Ypt7p:lipid, based on the number of Ypt7p molecules per cell, gives a Ypt7p:lipid molar ratio of ~1:5700, or ~500 Ypt7p molecules per μm^2 (Lo *et al.*, 2011), considerably higher than that of Zick *et al.* (2014) but still well below the ratio on our liposomes. Ypt7p is enriched at sites of vacuole tethering, but only twofold—though this is a lower bound for enrichment, since membrane bilayers are thinner than the effective resolution (~200 nm) of the epifluorescence microscopy used for these measurements (Wang *et al.*, 2002). We did not observe tethering when Ypt7p was incorporated at lower levels (unpublished data); this result has been seen previously (Hickey and Wickner, 2010). Thus the results we present here do not rule out—and indeed point to—the involvement of interactions between HOPS and other proteins and/or lipids that contribute to Ypt7p-and HOPS-mediated membrane tethering. One possibility is the AP-3 cargo adapter subunit Apl5p, which binds HOPS via its Vps41p subunit (Angers and Merz, 2009).

We next measured the size of our liposomes. By dynamic light scattering (DLS; see *Materials and Methods*), liposomes, whether Ypt7p incorporated or mock treated with the Ypt7p buffer, were always 110–125 nm in diameter (Figure 1B). Polydispersity was moderate (15–25%; Figure 1B). By cryo-electron microscopy (Figure 1C), mean liposome diameter was ~82 nm. (Hydration may account for the difference in values measured by these techniques.) Thus our liposomes are good models for large organelles, for example, MVBs/late endosomes, which have diameters of 100–150 nm (Nickerson *et al.*, 2006), and yeast vacuoles, which are 2–3 μm in diameter (Indge, 1968).

We then measured tethering of liposomes using confocal fluorescence microscopy. Light microscopy cannot resolve individual liposomes as small as the ones used here (Figure 1B). To overcome this limitation, we detected tethering by evaluating colocalization of two sets of liposomes, one labeled with lipid-conjugated fluorescein and the other labeled with lipid-conjugated Texas Red (Figures 2A and 3A). We quantified colocalization, and thus membrane tethering, by calculating a Pearson's correlation coefficient for the red and green channels of images of tethering reactions (Manders *et al.*, 1993; see *Materials and Methods*). All the correlation coefficients reported here are averages from three whole fields of view from one of at least three experiments using different preparations of liposomes (Figures 2B and 3B). The images displayed here were adjusted, with linear modifications only, for optimal viewing of green and red (shown as magenta) channels. We calculated correlation coefficients, however, from images that were unmodified except for conversion from 16-bit to 8-bit pixel depth.

We first asked whether Ypt7p is needed on zero, one, or two membranes for HOPS-mediated tethering. We saw no tethering in the absence of HOPS (Figure 2, A, column 1, and B). We also saw no tethering when Ypt7p was not on either set of liposomes (Figure 2, A, row a, and B). When Ypt7p was present on just one set of liposomes, HOPS induced clustering only for that population (Figure 2A, rows b and c). Correspondingly, correlation coefficients were 0.0013 when Ypt7p was present on Texas Red–labeled

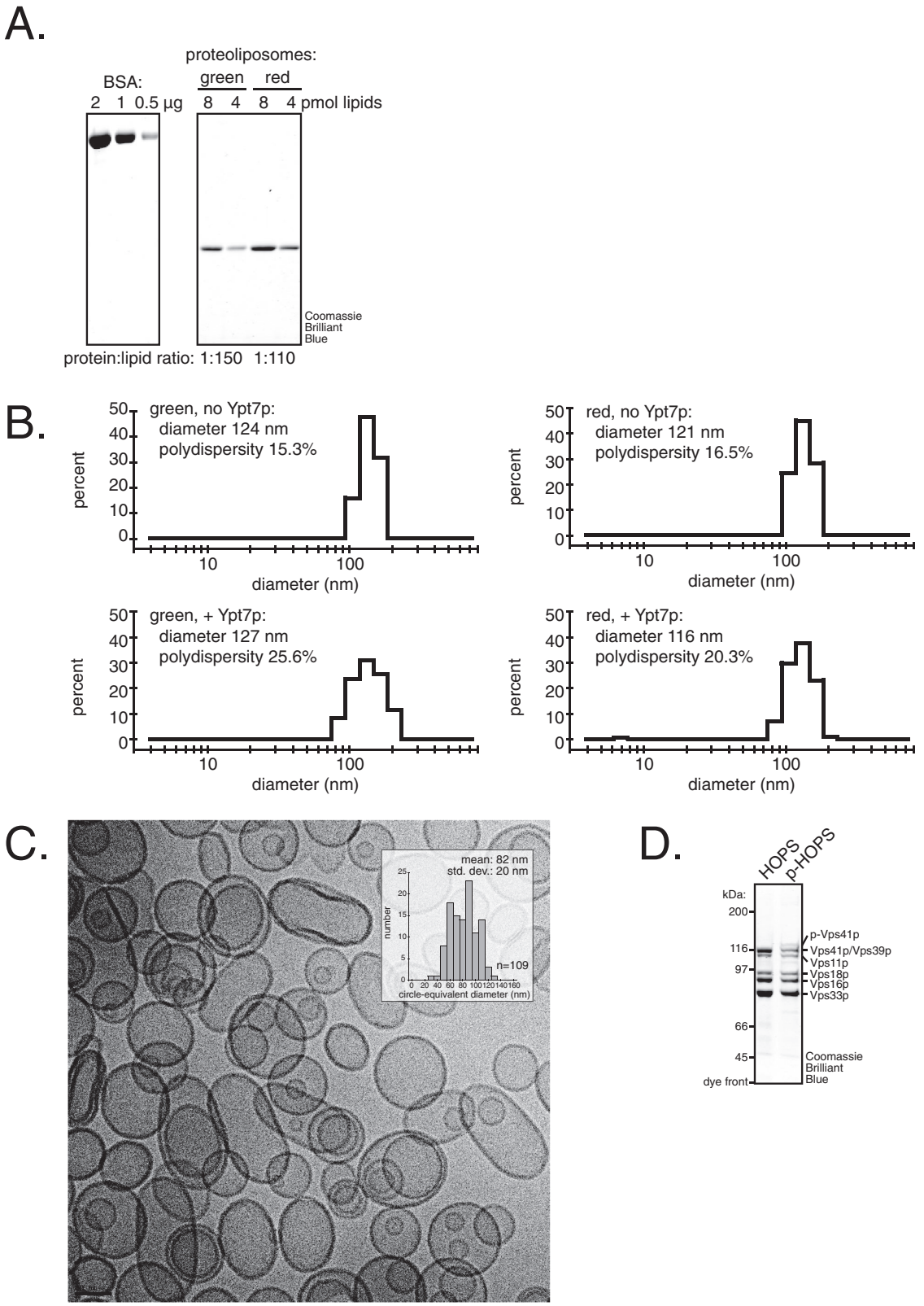

FIGURE 1: Characterization of reagents. (A) Ypt7p incorporation into proteoliposomes. Left panel, BSA standard; right panel, proteoliposomes. The two panels are from a single scan of a single SDS–PAGE gel. (B) Histograms of size distributions of typical liposome preparations, measured by dynamic light scattering and displayed at optimal resolution. (C) Cryo-electron microscopic image of liposomes bearing Ypt7p. Scale bar: 50 nm. Inset, histogram of circle-equivalent diameters (see *Materials and Methods*). (D) HOPS phosphorylation by Yck3p.

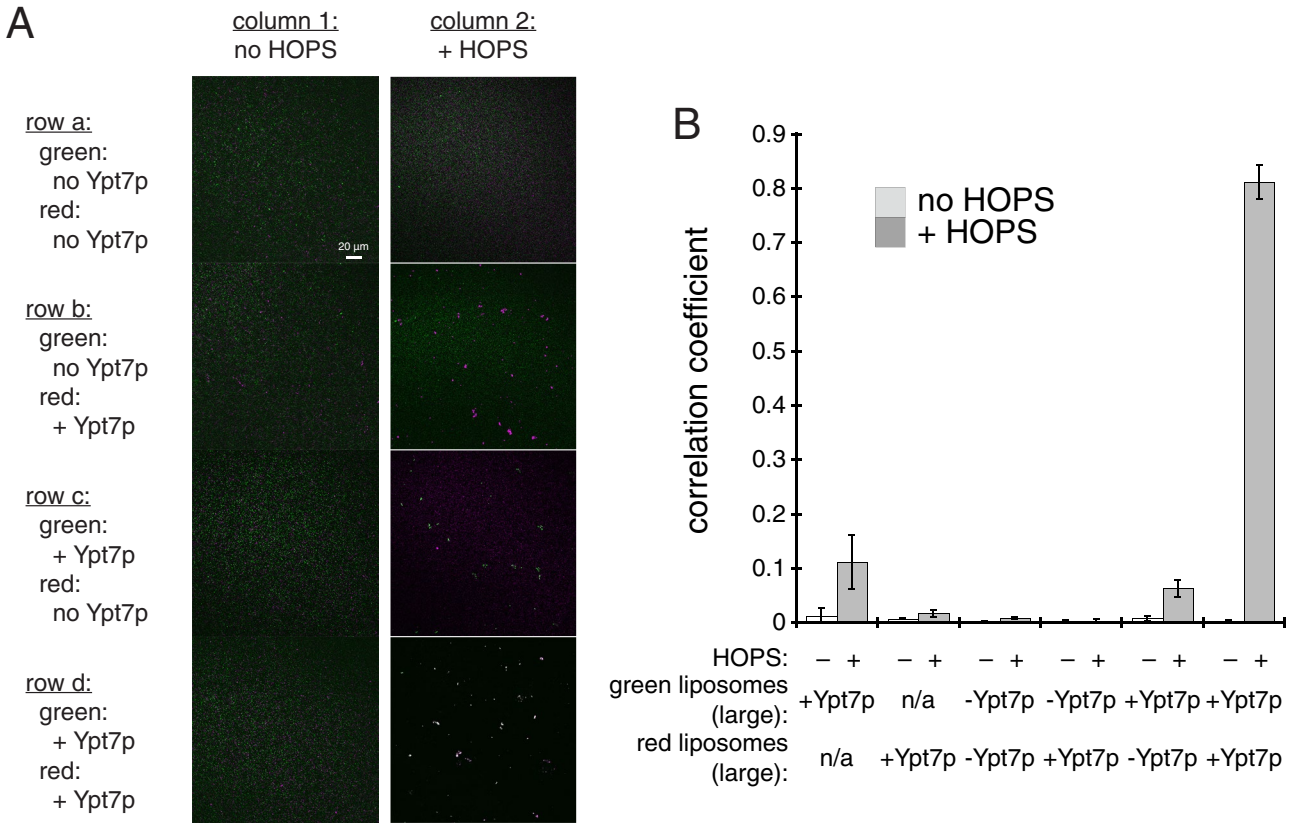

FIGURE 2: Ypt7p is required on two low-curvature membranes for tethering by HOPS. (A) Representative overlays of red (shown as magenta) and green channels for images of the indicated tethering reactions. Whole fields of view are shown. For optimal viewing only, magenta and green channels were independently adjusted using linear adjustments only. (B) Pearson's correlation coefficients for red and green channels of images of the indicated tethering reactions, calculated from unmodified (except for conversion from 16-bit to 8-bit) images using the JaCoP plug-in in ImageJ. Single-color images (corresponding to the first four bars) were used to estimate the contribution of bleed-through to apparent colocalization (see *Materials and Methods*).

liposomes only, and 0.063 when Ypt7p was present only on fluorescein-labeled liposomes (Figure 2B). We observed HOPS-mediated tethering of fluorescein-and Texas Red–labeled liposomes only when Ypt7p was on both populations (Figure 2, A, row d, and B; correlation coefficient 0.81). Thus, HOPS-mediated tethering of low-curvature membranes requires Ypt7p to be present in both membranes.

We next asked whether HOPS-mediated tethering was specific for the nucleotide state of Ypt7p. We loaded Ypt7p with either GDP or GTP (see *Materials and Methods*), then incorporated these proteins into liposomes labeled with fluorescein or Texas Red. Ypt7p-GDP and Ypt7p-GTP were incorporated into liposomes at roughly the same levels (unpublished data). Here we also saw that membranes lacking Ypt7p did not tether (Figure 3A, row a). When either Ypt7p-GDP or Ypt7p-GTP was present in one set of liposomes, HOPS tethered that set of liposomes only (Figure 3A, rows b–d and g). In contrast, when Ypt7p-GDP or Ypt7p-GTP was present in both fluorescein-and Texas Red–labeled liposomes, HOPS tethered both sets of liposomes together (Figure 3A, rows e, f, h, and i). Correlation coefficients for these images support these conclusions (Figure 3B): correlation coefficients were between 0.005 and 0.015 when Ypt7p was on one set of liposomes, whereas correlation coefficients were 0.5–0.85 when Ypt7p was on both. HOPS had a slight preference for tethering liposomes with Ypt7p-GTP over liposomes with Ypt7p-GDP: the mean cross-sectional area occupied by clusters of liposomes containing only Ypt7p-GTP was 2.0 ± 0.16 μm^2, whereas the mean cross-sectional area occupied by clusters of liposomes bearing only Ypt7p-GDP was 0.76 ± 0.042 μm^2 (see *Materials and Methods*). Nevertheless, correlation coefficients clearly show that HOPS tethers liposomes containing Ypt7p-GDP efficiently, for example, when Ypt7p-GDP is present on both fluorescein-and Texas Red–labeled liposomes (Figure 3B).

We therefore investigated the effect of HOPS phosphorylation by the vacuolar casein kinase I, Yck3p. Phosphorylation of HOPS by Yck3p confers specificity of HOPS for binding to Ypt7p-GTP over Ypt7p-GDP and for fusion of liposomes bearing Ypt7p-GTP versus liposomes bearing Ypt7p-GDP (Zick and Wickner, 2012). HOPS phosphorylation also inhibits membrane binding by the curvature-sensing amphipathic lipid–packing sensor (ALPS) motif on Vps41p (Cabrera *et al.*, 2010); Yck3p thereby down-regulates HOPS activity during hyperosmotic shock (LaGrassa and Ungermann, 2005). The liposomes we used here, with a diameter of 80–120 nm (Figure 1, B and C), were too large for HOPS to recognize via its ALPS motif, which has a strong preference for liposomes of diameter 60 nm or less (Cabrera *et al.*, 2010). Thus we could test here the effect of HOPS phosphorylation on the nucleotide specificity of HOPS-mediated tethering only. We phosphorylated HOPS in vitro, using purified recombinant Yck3p (Hickey *et al.*, 2009; see *Materials and Methods*). We then detected phosphorylation by a decrease in the electrophoretic mobility of Vps41p (Figure 1D). (Western blot

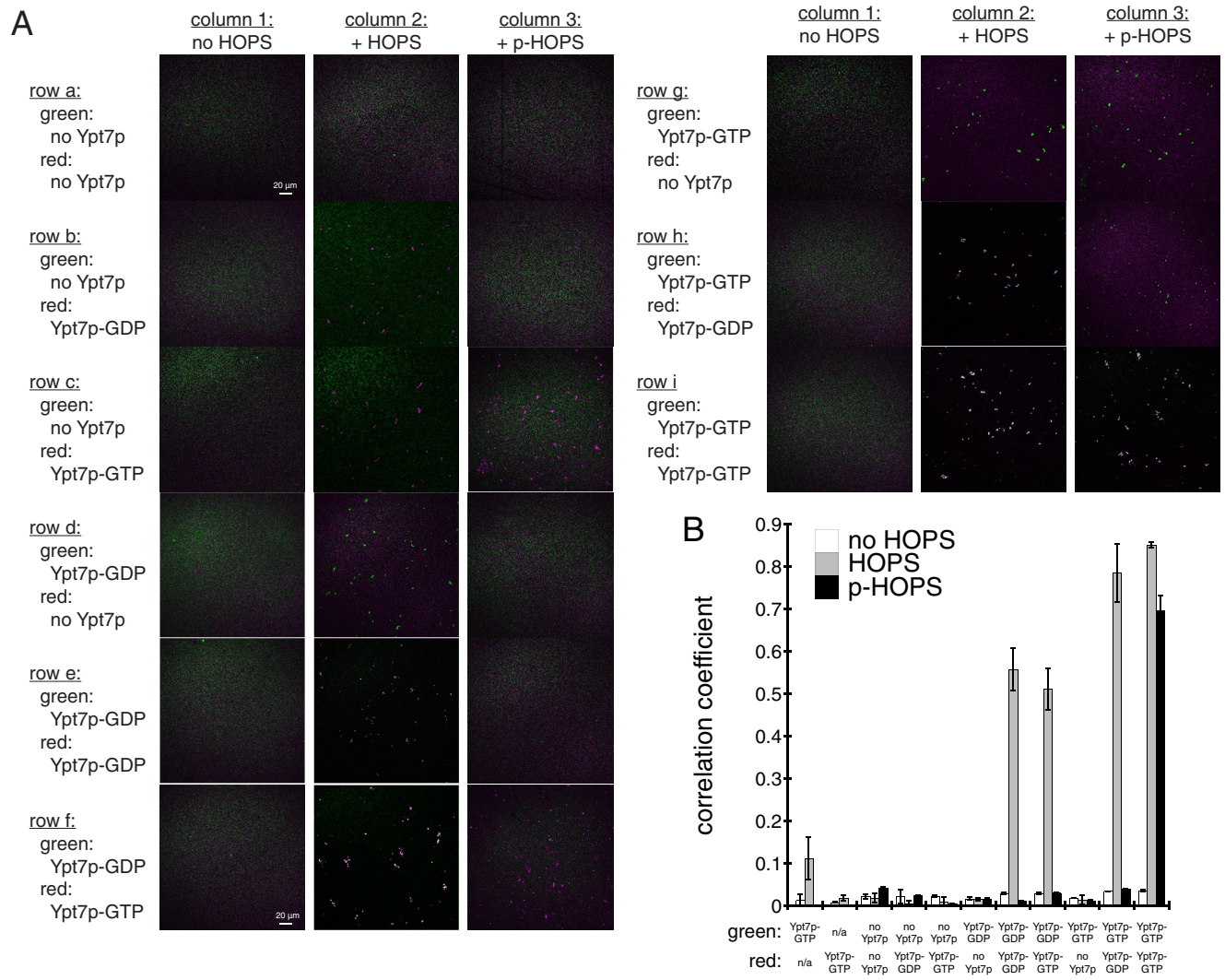

FIGURE 3: Phosphorylation of HOPS by Yck3p generates a requirement for Ypt7p-GTP on two membranes for tethering. (A) Representative overlays of red (shown as magenta) and green channels for images of the indicated tethering reactions. Whole fields of view are shown. For optimal viewing only, magenta and green channels were independently adjusted using linear adjustments only. (B) Pearson's correlation coefficients for red and green channels of images of the indicated tethering reactions, calculated from unmodified (except for conversion from 16-bit to 8-bit) images using the JaCoP plug-in in ImageJ. Single-color images (corresponding to the first 4 bars) were used to estimate the contribution of bleed-through to apparent colocalization (see *Materials and Methods*).

analysis has shown that Vps41p is the only HOPS subunit with altered gel mobility upon phosphorylation [Collins *et al.*, 2005].)

HOPS phosphorylation by Yck3p conferred strict nucleotide specificity for HOPS-mediated membrane tethering, just as seen by Zick and Wickner (2012). When liposomes were incubated with phosphorylated HOPS (p-HOPS), we saw membrane tethering only for liposomes bearing Ypt7p-GTP (Figure 3A, column 3, rows c and f–i). This was true even when liposomes bearing Ypt7p-GTP were mixed with liposomes bearing Ypt7p-GDP: in the presence of unphosphorylated HOPS, liposomes bearing Ypt7p-GTP tethered with liposomes bearing Ypt7p-GDP, whereas only clusters of the liposomes bearing Ypt7p-GTP were observed in the presence of p-HOPS (Figure 3A, rows f and h; compare columns 2 and 3). Accordingly, for mixtures of Ypt7p-GTP and Ypt7p-GDP liposomes, correlation coefficients were between 0.5 and 0.8 in the presence of HOPS but were close to zero in the presence of p-HOPS (Figure 3B). This requirement for Ypt7p-GTP on both membranes for tethering by p-HOPS exactly mirrors the requirement for Ypt7p-GTP on both membranes for membrane fusion catalyzed by p-HOPS (Zick and Wickner, 2012).

Our data provide the first experimental evidence for the proposal that phosphorylation of HOPS by the vacuolar casein kinase I, Yck3p, generates a requirement for Ypt7p-GTP in *both* apposed membranes for tethering of low-curvature membranes (Brett *et al.*, 2008). Placing our results in their physiological context, then, we propose that two events must take place before tethering of MVBs/late endosomes at vacuoles (Figure 4A). First, MVB-and vacuole-associated Ypt7p must both be exchanged into their GTP-bound state by the guanine nucleotide exchange factor (GEF) for Ypt7p, the Ccz1p-Mon1p complex (Nordmann *et al.*, 2010). This is consistent with the finding that Ccz1p-Mon1p is primarily found on MVBs, but also on vacuoles (Nordmann *et al.*, 2010; Lawrence *et al.*, 2014). Second, vacuole-associated HOPS must be phosphorylated on its Vps41p subunit by Yck3p (LaGrassa and Ungermann, 2005). Mon1p also is phosphorylated by Yck3p, which causes release of Mon1p (and presumably Ccz1p) from

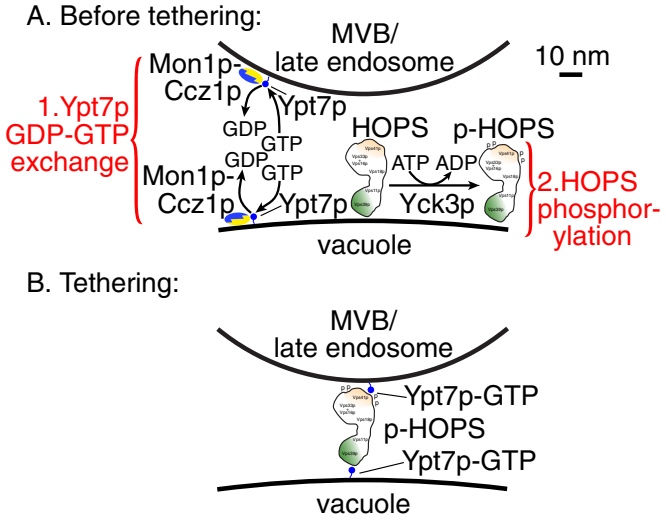

FIGURE 4: Model for Ypt7p-and HOPS-dependent membrane tethering. (A) Events before tethering per se: 1. Ypt7p nucleotide exchange, catalyzed by Ccz1p-Mon1p, on both MVB/late endosome and vacuole membrane. (For homotypic vacuole tethering, nucleotide exchange similarly must occur on both membranes.) 2. Phosphorylation of HOPS by Yck3p. (B) Membrane tethering by p-HOPS, binding to a molecule of Ypt7p-GTP in each apposed membrane.

vacuoles (Lawrence *et al.*, 2014); this may allow redistribution of Ccz1p-Mon1p to MVBs after fusion of MVBs with vacuoles. Finally, we propose that phosphorylated HOPS tethers membranes (Figure 4B) by binding to one molecule of Ypt7p-GTP on each membrane via its two Ypt7p binding sites, on Vps41p and on Vps39p (Wurmser *et al.*, 2000; Brett *et al.*, 2008; Bröcker *et al.*, 2012). In our model, homotypic tethering of vacuoles also has the same requirement for Ypt7p-GTP on both tethered membranes and also is mediated by simultaneous binding of p-HOPS to Ypt7p-GTP in each membrane.

MATERIALS AND METHODS

Protein purification

HOPS complex (Zick and Wickner, 2013), Ypt7p (Stroupe *et al.*, 2009), and Yck3p (Hickey *et al.*, 2009) were expressed and purified as previously described.

HOPS phosphorylation

We phosphorylated purified HOPS in a 1 ml reaction containing 1 μM HOPS, 100 nM Yck3p, 1 mM $MgCl_2$, and 0.5 mM ATP in HOPS buffer (20 mM NaHEPES, pH 7.4, 400 mM NaCl, 10% vol/vol glycerol, 5 mM β-mercaptoethanol, and 0.004% Triton X-100) at 4°C for 10 h. We then separated p-HOPS from Yck3p by size-exclusion chromatography in a 21-ml (1 cm × 27 cm) Sephacryl S-300 column equilibrated in HOPS buffer (flow rate 0.5 ml/min.). This p-HOPS was frozen in small aliquots in liquid N_2 and stored at −80°C

Nucleotide exchange on Ypt7p

Ypt7p was nucleotide exchanged in a modification of a previously reported procedure (Zick and Wickner, 2012). We incubated 100–200 μl of purified Ypt7p, at 50–100 μM, with 1 mM GTP or GDP (sodium salts; Sigma-Aldrich, St. Louis, MO) and 2.5 mM Na_2EDTA for 30 min on ice, then added $MgCl_2$ to a final concentration of 5 mM and incubated the mixture for a further 15 min on ice. This Ypt7p was then immediately incorporated into liposomes, as described below.

Liposome preparation

All lipids were from Avanti Polar Lipids (Alabaster, AL), except for fluorophore-conjugated lipids, which were from Molecular Probes/Life Technologies (Grand Island, NY).

A mixture of POPC (95.5 mol%), POPS (4.4 mol%), and either Texas Red–DHPE (0.1 mol%) or fluorescein-DHPE (0.1 mol%) was dried under a stream of argon gas in a 50-ml pear-shaped flask. This lipid film was dissolved in diethyl ether to a concentration of 10 mM lipids. An equal volume of RB150 (20 mM NaHEPES, pH 7.4, 150 mM NaCl, 10% vol/vol glycerol) was added, and the biphasic mixture was bath sonicated for 30–60 s, until it became a stable emulsion. The flask containing this emulsion was then placed on a rotary evaporator and subjected to a vacuum that was, over 60 min, gradually increased to 80 kPa below atmospheric pressure. The flask was then flushed with argon gas and placed on the rotary evaporator at 80 kPa below atmospheric pressure for 30 min to remove all detectable traces of organic solvent. The lipid suspension was then subjected to 15 passes through an Avestin (Ottawa, ON, Canada) LiposoFast extruder fitted with a Nuclepore polycarbonate membrane with 100-nm pore size (GE Healthcare, Piscataway, NJ). The resulting suspension contained large vesicles with a hydrodynamic diameter of between 100 and 120 nm, as confirmed by dynamic light scattering.

POPS was necessary to prevent irreversible aggregation of large liposomes during preparation. The mole percent of POPS that we used, 4.4%, is equal to that measured in purified vacuoles (Zinser *et al.*, 1991). Given the affinity of HOPS for negatively charged lipids (Stroupe *et al.*, 2006), POPS would favor HOPS association and thus tethering of POPS-containing membranes even in the absence of Ypt7p. However, we found that Ypt7p was always required in all POPS-containing liposomes in order for these membranes to tether (Figures 2 and 3).

Lipid concentration measurement

Lipid concentrations were measured using the ammonium molybdate/ascorbic acid assay for lipid phosphorus, as described previously (Zick *et al.*, 2014).

Ypt7p incorporation

Ypt7p was incorporated into liposomes at a molar protein:lipid ratio of 1:100 via the "direct" incorporation method (Rigaud and Levy, 2003). Liposomes (1 μmol lipids) were mixed with 10 nmol nucleotide-exchanged Ypt7p (dissolved in RB150 with 34.2 mM [1% wt/vol] *n*-β-octylglucopyranoside [βOG] and excess nucleotide, $MgCl_2$, and EDTA, as described above) and RB150 + 1 mM $MgCl_2$ such that the final concentration of βOG was 10 mM. (In a typical incorporation reaction, 50 μl of liposomes at 2 mM lipids was mixed with 290 μl RB150 + 1 mM $MgCl_2$ and 140 μl Ypt7p at 70 μM.) This [βOG] is well below its critical micelle concentration of ~20–25 mM. Nevertheless, no precipitation of Ypt7p was ever observed, and we routinely obtained essentially quantitative yields of Ypt7p in our recovered liposomes (Figure 1A). For preparing liposomes without Ypt7p, the Ypt7p solution was replaced by an equal volume of RB150 + 1 mM $MgCl_2$ + 34.2 mM (1%) βOG. Incorporation reactions were incubated at room temperature for 1 h and then dialyzed in 20-kDa cutoff Slide-A-Lyzer dialysis units (0.5–3 ml capacity; Thermo Scientific Pierce, Rockford, IL) against 2 l RB150 + 1 mM $MgCl_2$ overnight at 4°C with ~0.5 g Bio-Beads SM-2 (Bio-Rad, Hercules, CA) outside the dialysis membranes. Buffer was changed once after 3–4 h, and fresh Bio-Beads were added at this time. Dialyzed incorporation reactions were mixed with an equal volume of 80% Histodenz (Sigma-Aldrich) in RB150 + 1 mM $MgCl_2$, placed in ultracentrifuge tubes (11 × 60 mm; Beckman, Indianapolis, IN) and overlaid with 1 ml 30%

Histodenz in RB150 + 1 mM $MgCl_2$, then with sufficient RB150 + 1 mM $MgCl_2$ to fill the tubes. Gradients were centrifuged in an SW-60 rotor (Beckman) at 50,000 rpm for 3 h at 4°C. Liposomes were harvested from the top interface of the gradients and dialyzed again as described above, except using 20-kDa cutoff Slide-A-Lyzer Mini dialysis units (Pierce) and without Bio-Beads. Liposome sizes were measured by dynamic light scattering (Figure 1B). Liposomes were stored at 4°C and were used within 2 d of being prepared.

Electron microscopy

For freezing liposomes, 1 µl of a liposome suspension (at 0.1 mM lipids in 20 mM NaHEPES, pH 7.4, 150 mM NaCl, 1 mM $MgCl_2$) was applied to glow-discharged C-flat holey carbon grids (Electron Microscopy Sciences, Hatfield, PA). Excess liquid was briefly wicked away using 3-mm Chr Whatman filter paper, and grids were immediately plunged into liquid ethane in a bath of liquid nitrogen. Grids were stored at liquid nitrogen temperatures and imaged using an FEI Tecnai F20 electron microscope. Areas occupied by liposomes were measured using the ellipse tool in ImageJ. Circle-equivalent diameters (i.e., the diameter of a circle with the same area as the ellipse) were then calculated using the following formula: diameter $= (4 \times \text{area}/\pi)^{0.5}$.

Tethering reactions

Tethering reactions contained 50 µM each of Texas Red– and fluorescein-labeled lipids. Liposomes were mixed together and brought to a volume of 20 µl with RB150 + 1 mM $MgCl_2$. To this mixture was added 5 µl of HOPS complex (50 nM final) or HOPS buffer. The reaction was incubated at room temperature for 45 min. A portion (5 µl) of the reaction was then placed on a glass microscope slide and covered with a cover glass.

Confocal microscopy and image analysis

Tethering reactions were imaged using an inverted Olympus (Center Valley, PA) Fluoview 300 laser-scanning confocal microscope in sequential-scanning mode. The focal plane was just above the cover glass. Slides and cover glasses were not cleaned; when we did apply a cleaning protocol (Domanska *et al.*, 2009), liposomes fused with the glass, and clusters were disrupted (unpublished data). Fluorescein was excited using a 488-nm Melles-Griot (Carlsbad, CA) argon ion laser and detected using a 505- to 525-nm band-pass filter. Texas Red was excited using a 543-nm Melles-Griot helium–neon laser and detected using a 578- to 623-nm band-pass filter. The objective was an Olympus (Shinjuku-ku, Tokyo, Japan) Plan-Apo N 60×/1.45 TIRFM oil-immersion lens. Images were acquired using a photomultiplier tube (PMT).

To ensure that misregistration did not bias our analysis, especially for reactions in which little or no tethering occurred, that is, in which there was little apparent colocalization of red and green liposomes, we imaged four-color fluorescent beads (0.1-µm Tetraspeck fluorescent microspheres; Molecular Probes/Life Technologies) and evaluated the colocalization of red and green fluorescent signals using line scans in ImageJ (Supplemental Figure 1). In no case were the peaks corresponding to the red and green signals from individual fluorescent beads offset by more than one pixel in our images. This corresponds to a 230.2-nm offset, or only a little larger than the maximum theoretical optical resolution of our system, given the wavelengths and objective lens that we used here: if we assume fluorescein emission is at the center of the wavelengths passed by the filter for the green channel (see above), then $R = \lambda/2\text{NA} = 515$ nm/2.9 = 178 nm. Thus, while it is theoretically possible that two liposomes could be colocalized and yet have their signals assigned to different pixels due to misregistration, line-scan analysis of tethered liposome clusters (Supplemental Figure 2) shows that under the reaction conditions used here, essentially all tethered liposomes entered into very large clusters. Thus it is unlikely that a significant number of undetected small liposome clusters are present in our tethering reactions.

Images were separated into green and red channels using ImageJ. Pearson's correlation coefficients between green and red channels were calculated using the JaCoP plug-in in ImageJ. The images used for Pearson's coefficient calculation were converted from 16-bit to 8-bit pixel depth but were not otherwise altered. In Figures 2B and 3B we report averages and SDs for Pearson's correlation coefficients calculated from three images of each reaction. The full field of view was used for calculations; representative fields among those used for calculations are shown in Figures 2A and 3A. Each experiment was repeated at least three times using different preparations of liposomes.

Pearson's correlation coefficients are sensitive only to the spatial distribution of pixels, not to the average value of pixel intensities in an image (Manders *et al.*, 1993). Nevertheless, we wanted to ensure that our analysis was not skewed by an excess of saturated pixels, because in a tethered cluster, several liposomes are likely to be present in the region corresponding to a single pixel in an image, which could (and did) result in very bright pixels. At the same time, we wanted to avoid underexposing images of reactions containing mostly untethered liposomes. Thus, for both green and red channels, we collected images using two different settings for laser intensity and PMT parameters: a "low" setting that was optimized for tethered clusters and a "high" setting optimized for untethered liposomes. These settings were obtained by adjusting laser intensity and PMT parameters until images of single-color clusters (made by incubating Ypt7p-GTP–bearing liposomes with HOPS) and images of untethered liposomes (made by incubating the same Ypt7p-GTP-bearing liposomes with HOPS buffer only) each contained only a few saturated pixels (not more than ~1000, i.e., 0.1% of a 1024 pixel by 1024 pixel image). We made these measurements independently at the beginning of each experiment. However, the settings we used were always roughly equal to the following: for detecting fluorescein, laser power 15%, PMT gain 1.3, and offset 3%, and for the "high" setting PMT voltage 851, while for the "low" setting PMT voltage 701; for detecting Texas Red, laser power 15%, PMT gain 1.5, and offset 5%, and for the "high" setting PMT voltage 725, while for the "low" setting PMT voltage 575.

We calculated Pearson's correlation coefficients from pairs of images collected using the optimal settings for the level of clustering in that image, as assessed by visual inspection. That is, we used images collected under the "high" setting for nonclustered liposomes and images collected under the "low" setting for clustered liposomes. We did this even when the two differently colored populations of liposomes in a single tethering reaction had different behavior; for example, for mixtures of fluorescein-labeled liposomes without Ypt7p and Texas Red–labeled liposomes with Ypt7p (Figure 2A, row b), we used the "high" setting. While this was a potential source of bias, it was readily apparent in every image whether clusters or individual liposomes were predominant (Figures 2A and 3A).

To assess the degree to which "bleed-through," or detection of fluorescein in the red channel and detection of Texas Red in the green channel, contributed to apparent colocalization, we collected images of single-color untethered liposomes in both green and red channels; we also did this for single-color clusters prepared by

addition of HOPS to Ypt7p-bearing fluorescein-or Texas Red–labeled liposomes. As shown in Figures 2B and 3B, images of untethered liposomes and clusters of Texas Red–labeled liposomes had correlation coefficients between red and green channels essentially equal to zero. However, clusters of fluorescein-labeled liposomes had a correlation coefficient of ~0.1 between red and green channels (Figures 2B and 3B). This is the expected result, based on the wavelengths of the lasers used for excitation and the band-pass filters used for detection and the fact that clusters of liposomes contain a higher local concentration of liposomes than untethered liposomes and thus give rise to a stronger fluorescence signal. Thus a correlation coefficient of 0.1 represents the lower limit of colocalization we can detect by the methods used here.

Statistical analysis of the distributions of pixel intensities in images with or without significant tethering is shown in Supplemental Figure 3. Here we found that clustering, as expected, caused an increase in the "rightward" skew of the intensity distribution, that is, toward higher pixel intensities. Intensity distributions also were "sharper" when tethering occurred, due to a relatively smaller number of pixels with moderate intensities. This led to increased skewness and kurtosis parameters for images with clustered liposomes (Supplemental Figure 3).

HOPS dose-response and time-course analysis for tethering are shown in Supplemental Figure 4.

For calculation of mean cluster areas, unmodified images were thresholded using the Maximum Entropy method in ImageJ (Kapur *et al.*, 1985). Cluster areas then were measured using ImageJ. Mean cluster areas were calculated from at least three images.

For visual display of representative images only, brightness and contrast of red and green channels were modified independently in Adobe Photoshop, using linear adjustments only.

Note added in proof. It has come to our attention that the vacuolar lipid:protein ratios reported in Table 1 of Zick *et al*. (2014) were, due to a typographical error, 10 times higher than the ratios that in fact were measured. The lipid:Ypt7p ratio actually measured by Zick *et al*. (2014) was ~2×10^4, which corresponds to ~125 Ypt7p molecules per μm^2, much closer to the value (~500 Ypt7p molecules per μm^2) estimated by Lo *et al*. (2011).

ACKNOWLEDGMENTS

We gratefully acknowledge Avril Somlyo (University of Virginia, Charlottesville, VA) for access to the confocal microscope and Zygmunt Derewenda (University of Virginia School of Medicine) for access to the DynaPro Titan. Cryo-EM work, for which we thank Kelly Dryden, was done at the Molecular Electron Microscopy Core at the University of Virginia, supported by the University of Virginia School of Medicine and built with a National Institutes of Health grant (G20-RR31199).

REFERENCES

Angers CG, Merz AJ (2009). HOPS interacts with Apl5 at the vacuole membrane and is required for consumption of AP-3 transport vesicles. Mol Biol Cell 20, 4563–4574.

Araç D, Chen X, Khant HA, Ubach J, Ludtke SJ, Kikkawa M, Johnson AE, Chiu W, Sudhof TC, Rizo J (2006). Close membrane-membrane proximity induced by Ca^{2+}-dependent multivalent binding of synaptotagmin-1 to phospholipids. Nat Struct Mol Biol 13, 209–217.

Bonifacino JS, Hierro A (2011). Transport according to GARP: receiving retrograde cargo at the trans-Golgi network. Trends Cell Biol 21, 159–167.

Brett CL, Plemel RL, Lobingier BT, Vignali M, Fields S, Merz AJ (2008). Efficient termination of vacuolar Rab GTPase signaling requires coordinated action by a GAP and a protein kinase. J Cell Biol 182, 1141–1151.

Bröcker C, Kuhlee A, Gatsogiannis C, Balderhaar HJ, Honscher C, Engelbrecht-Vandre S, Ungermann C, Raunser S (2012). Molecular architecture of the multisubunit homotypic fusion and vacuole protein sorting (HOPS) tethering complex. Proc Natl Acad Sci USA 109, 1991–1996.

Burke LI, Patil GS, Panganamala RV, Geer JC, Cornwell DG (1973). Surface areas of naturally occurring lipid classes and the quantitative microdetermination of lipids. J Lipid Res 14, 9–15.

Cabrera M, Langemeyer L, Mari M, Rethmeier R, Orban I, Perz A, Bröcker C, Griffith J, Klose D, Steinhoff HJ, *et al*. (2010). Phosphorylation of a membrane curvature-sensing motif switches function of the HOPS subunit Vps41 in membrane tethering. J Cell Biol 191, 845–859.

Calero M, Chen CZ, Zhu W, Winand N, Havas KA, Gilbert PM, Burd CG, Collins RN (2003). Dual prenylation is required for Rab protein localization and function. Mol Biol Cell 14, 1852–1867.

Collins KM, Thorngren NL, Fratti RA, Wickner WT (2005). Sec17p and HOPS, in distinct SNARE complexes, mediate SNARE complex disruption or assembly for fusion. EMBO J 24, 1775–1786.

Cottam NP, Wilson KM, Ng BG, Korner C, Freeze HH, Ungar D (2014). Dissecting functions of the conserved oligomeric Golgi tethering complex using a cell-free assay. Traffic 15, 12–21.

Domanska MK, Kiessling V, Stein A, Fasshauer D, Tamm LK (2009). Single vesicle millisecond fusion kinetics reveals number of SNARE complexes optimal for fast SNARE-mediated membrane fusion. J Biol Chem 284, 32158–32166.

Drin G, Morello V, Casella JF, Gounon P, Antonny B (2008). Asymmetric tethering of flat and curved lipid membranes by a golgin. Science 320, 670–673.

Garg S, Sharma M, Ung C, Tuli A, Barral DC, Hava DL, Veerapen N, Besra GS, Hacohen N, Brenner MB (2011). Lysosomal trafficking, antigen presentation, and microbial killing are controlled by the Arf-like GTPase Arl8b. Immunity 35, 182–193.

Grosshans BL, Ortiz D, Novick P (2006). Rabs and their effectors: achieving specificity in membrane traffic. Proc Natl Acad Sci USA 103, 11821–11827.

Heider MR, Munson M (2012). Exorcising the exocyst complex. Traffic 13, 898–907.

Hickey CM, Stroupe C, Wickner W (2009). The major role of the Rab Ypt7p in vacuole fusion is supporting HOPS membrane association. J Biol Chem 284, 16118–16125.

Hickey CM, Wickner W (2010). HOPS initiates vacuole docking by tethering membranes before trans-SNARE complex assembly. Mol Biol Cell 21, 2297–2305.

Indge KJ (1968). The isolation and properties of the yeast cell vacuole. J Gen Microbiol 51, 441–446.

Kapur JN, Sahoo PK, Wong AKC (1985). A new method for gray-level picture thresholding using the entropy of the histogram. Comput Vision Graph 29, 273–285.

LaGrassa TJ, Ungermann C (2005). The vacuolar kinase Yck3 maintains organelle fragmentation by regulating the HOPS tethering complex. J Cell Biol 168, 401–414.

Lawrence G, Brown CC, Flood BA, Karunakaran S, Cabrera M, Nordmann M, Ungermann C, Fratti RA (2014). Dynamic association of the PI3P-interacting Mon1-Ccz1 GEF with vacuoles is controlled through its phosphorylation by the type 1 casein kinase Yck3. Mol Biol Cell 25, 1608–1619.

Lo SY, Brett CL, Plemel RL, Vignali M, Fields S, Gonen T, Merz AJ (2011). Intrinsic tethering activity of endosomal Rab proteins. Nat Struct Mol Biol 40–49.

Lobingier BT, Merz AJ (2012). Sec1/Munc18 protein Vps33 binds to SNARE domains and the quaternary SNARE complex. Mol Biol Cell 23, 4611–4622.

Manders EMM, Verbeek FJ, Aten JA (1993). Measurement of colocalization of objects in dual-color confocal images. J Microsc-Oxford 169, 375–382.

Mayer A, Wickner W (1997). Docking of yeast vacuoles is catalyzed by the Ras-like GTPase Ypt7p after symmetric priming by Sec18p (NSF). J Cell Biol 136, 307–317.

Meiringer CT, Rethmeier R, Auffarth K, Wilson J, Perz A, Barlowe C, Schmitt HD, Ungermann C (2011). The Dsl1 protein tethering complex is a resident endoplasmic reticulum complex, which interacts with five soluble NSF (*N*-ethylmaleimide-sensitive factor) attachment protein receptors (SNAREs): implications for fusion and fusion regulation. J Biol Chem 286, 25039–25046.

Munro S (2011). The golgin coiled-coil proteins of the Golgi apparatus. Cold Spring Harbor Perspect Biol 3, a005256.

Nickerson DP, West M, Odorizzi G (2006). Did2 coordinates Vps4-mediated dissociation of ESCRT-III from endosomes. J Cell Biol 175, 715–720.
Nordmann M, Cabrera M, Perz A, Bröcker C, Ostrowicz C, Engelbrecht-Vandre S, Ungermann C (2010). The Mon1-Ccz1 complex is the GEF of the late endosomal Rab7 homolog Ypt7. Curr Biol 20, 1654–1659.
Novick P, Medkova M, Dong G, Hutagalung A, Reinisch K, Grosshans B (2006). Interactions between Rabs, tethers, SNAREs and their regulators in exocytosis. Biochem Soc Trans 34, 683–686.
Pfeffer SR (2001). Rab GTPases: specifying and deciphering organelle identity and function. Trends Cell Biol 11, 487–491.
Price A, Seals D, Wickner W, Ungermann C (2000). The docking stage of yeast vacuole fusion requires the transfer of proteins from a *cis*-SNARE complex to a Rab/Ypt protein. J Cell Biol 148, 1231–1238.
Rigaud JL, Levy D (2003). Reconstitution of membrane proteins into liposomes. Methods Enzymol 372, 65–86.
Sato TK, Rehling P, Peterson MR, Emr SD (2000). Class C Vps protein complex regulates vacuolar SNARE pairing and is required for vesicle docking/fusion. Mol Cell 6, 661–671.
Sönnichsen B, De Renzis S, Nielsen E, Rietdorf J, Zerial M (2000). Distinct membrane domains on endosomes in the recycling pathway visualized by multicolor imaging of Rab4, Rab5, and Rab11. J Cell Biol 149, 901–914.
Stroupe C, Collins KM, Fratti RA, Wickner W (2006). Purification of active HOPS complex reveals its affinities for phosphoinositides and the SNARE Vam7p. EMBO J 25, 1579–1589.
Stroupe C, Hickey CM, Mima J, Burfeind AS, Wickner W (2009). Minimal membrane docking requirements revealed by reconstitution of Rab GTPase-dependent membrane fusion from purified components. Proc Natl Acad Sci USA 106, 17626–17633.
Sztul E, Lupashin V (2006). Role of tethering factors in secretory membrane traffic. Am J Physiol Cell Physiol 290, C11–C26.
Tamura N, Mima J (2014). Membrane-anchored human Rab GTPases directly mediate membrane tethering in vitro. Biol Open 3, 1108–1115.
Walworth NC, Goud B, Kabcenell AK, Novick PJ (1989). Mutational analysis of SEC4 suggests a cyclical mechanism for the regulation of vesicular traffic. EMBO J 8, 1685–1693.
Wang L, Seeley ES, Wickner W, Merz AJ (2002). Vacuole fusion at a ring of vertex docking sites leaves membrane fragments within the organelle. Cell 108, 357–369.
Waters MG, Pfeffer SR (1999). Membrane tethering in intracellular transport. Curr Opin Cell Biol 11, 453–459.
Wickner W, Schekman R (2008). Membrane fusion. Nat Struct Mol Biol 15, 658–664.
Willett R, Ungar D, Lupashin V (2013). The Golgi puppet master: COG complex at center stage of membrane trafficking interactions. Histochem Cell Biol 140, 271–283.
Wurmser AE, Sato TK, Emr SD (2000). New component of the vacuolar class C-Vps complex couples nucleotide exchange on the Ypt7 GTPase to SNARE-dependent docking and fusion. J Cell Biol 151, 551–562.
Yu S, Liang Y (2012). A trapper keeper for TRAPP, its structures and functions. Cell Mol Life Sci 69, 3933–3944.
Zick M, Stroupe C, Orr A, Douville D, Wickner WT (2014). Membranes linked by *trans*-SNARE complexes require lipids prone to non-bilayer structure for progression to fusion. eLife 3, e01879 [correction published in eLife (2015), http://elifesciences.org/content/4/e08843].
Zick M, Wickner W (2012). Phosphorylation of the effector complex HOPS by the vacuolar kinase Yck3p confers Rab nucleotide specificity for vacuole docking and fusion. Mol Biol Cell 23, 3429–3437.
Zick M, Wickner W (2013). The tethering complex HOPS catalyzes assembly of the soluble SNARE Vam7 into fusogenic *trans*-SNARE complexes. Mol Biol Cell 24, 3746–3753.
Zinser E, Sperka-Gottlieb CD, Fasch EV, Kohlwein SD, Paltauf F, Daum G (1991). Phospholipid synthesis and lipid composition of subcellular membranes in the unicellular eukaryote *Saccharomyces cerevisiae*. J Bacteriol 173, 2026–2034.